2025 IEEE XVII International Scientific and Technical Conference on Actual Problems of Electronic Instrument Engineering (APEIE) | 979-8-3315-5916-8/25/$31.00 ©2025 IEEE | DOI: 10.1109/APEIE66761.2025.11289407

Proceedings of the

XVII International Scientific and Technical Conference «Actual Problems of Electronic Instrument Engineering»

APEIE

APEIE25
Actual Problems of Electronic Instrument Engineering

14–16 November 2025, Russia

IEEE Catalog Number: CFP25471-ART
ISBN: 979-8-3315-5916-8

2025 IEEE XVII International Scientific and Technical Conference on Actual Problems of Electronic Instrument Engineering (APEIE) | 979-8-3315-5916-8/25/$31.00 ©2025 IEEE | DOI: 10.1109/APEIE66761.2025.11289252

IEEE Catalog Number: CFP25471-ART
ISBN: 979-8-3315-5916-8

2025 IEEE XVII International Scientific and Technical Conference on Actual Problems of Electronic Instrument Engineering (APEIE) | 979-8-3315-5916-8/25/$31.00 ©2025 IEEE | DOI: 10.1109/APEIE66761.2025.11289266

Modelling the Effective Elastic Properties of Hydrate-Bearing Rocks: a Comparison of Static and Dynamic Approaches

Anastasiia Yu. Kutishcheva
Laboratory of mathematical modeling of multiphase processes in native and artificial multiscale heterogeneous media
Trofimuk Institute of Petroleum Geology and Geophysics of Siberian Branch Russian Academy of Sciences
Novosibirsk, Russia
KutischevaAY@ipgg.sbras.ru

***Abstract*—Accurate prediction of the elastic properties of hydrate-bearing sediments is crucial for seismic quantification and reservoir characterisation. This study investigates the relationship between static and dynamic elastic moduli in a synthetic three-component medium representing hydrate-bearing rock via finite element modelling. The digital rock model was constructed with a matrix of ordered packed quartz grains, a layer of methane hydrate coating the grains, and water-saturated pore space. A series of numerical experiments was performed where the hydrate saturation was systematically varied. For each configuration, two types of simulations were conducted: first, a static linear-elastic analysis to compute the effective static bulk and shear moduli under prescribed boundary conditions; second, a explicit dynamic wave propagation simulation to directly obtain the compressional (P-) and shear (S-) wave velocities. The results demonstrate that the P-wave velocities calculated from the static moduli using isotropic elastic theory show a remarkably high degree of agreement with the velocities derived from the dynamic wave simulation across the entire range of hydrate saturations. This strong correlation held when compared against available laboratory data. The findings confirm the adequacy of static numerical calculations as an efficient and reliable tool for predicting the dynamic elastic properties and seismic velocities of hydrate-bearing rocks, which can significantly streamline reservoir modelling workflows.**

Keywords—methane hydrate, effective elastic moduli, wave simulation, P-wave velocity, finite element method, digital rock physics.

I. INTRODUCTION

Methane hydrates are crystalline compounds that remain stable under specific conditions of high pressure and low temperature, representing a significant potential source of hydrocarbons [1], [2], [3]. Furthermore, their role in climate change issues and geological hazards necessitates the reliable prediction of their distribution and properties within natural reservoirs [1]. The primary method for the remote study of hydrate-bearing strata is seismic exploration, the interpretation of which directly depends on accurate rock physics models that link the elastic properties of rocks to their lithology, porosity, and saturation [3], [4], [5].

It is well-established that a discrepancy can exist between the static and dynamic elastic moduli of rocks, arising from effects such as non-linearity, scale effects, frequency dispersion, and the influence of microstructure [6]. For complex multi-component systems like hydrate-bearing rocks, this discrepancy requires careful examination. Traditional theoretical models (e.g., Hertz-Mindlin theory, Hashin-Shtrikman equations) and empirical approaches often prove insufficiently accurate for describing specific microstructures where hydrate cements the rock grains [7].

The advancement of computational methods, particularly Digital Rock Physics (DRP), offers a way to overcome these limitations by enabling the direct numerical simulation of physical processes on three-dimensional digital rock models. Both static (based on homogenization of static elastic moduli) and dynamic (based on wave propagation simulation) approaches are used in the literature [8], [9]. However, a direct comparison of these methods for three-component media with cementing hydrate, using identical digital models, has not been sufficiently addressed. This work is dedicated to verifying the correctness of calculating effective elastic wave velocities via static effective moduli for a three-component medium. The aim of the study is to compare two approaches:

- The indirect calculation of compressional (P-) and shear (S-) wave velocities using static effective moduli obtained by solving a stationary elastic problem.
- The direct calculation of P-wave velocity by solving a transient wave problem and recording the first-arrival time.

The relevance of this work lies in validating that less computationally intensive static calculations can be reliably used for constructing and evaluating the properties of rock physics models.

II. METHODOLOGY

A. Geometric Model and Material Properties

A synthetic three-component rock model (a cube with a 10 mm edge length) was developed (Fig. 1). The model consists of:

- quartz grains (spherical particles with a radius of 1.05 mm, packed in a regular cubic lattice to ensure macroscopic isotropy of the effective properties; perfect contact between grains is assumed),

- methane hydrate (a uniform layer on the surface of each quartz grain; within a single experiment, the layer thickness is constant),
- and water, which fills the remaining pore space.

The hydrate saturation was varied across a series of simulations solely by changing the hydrate layer thickness from 0.05 mm to 0.3 mm. This allowed for the investigation of the dependence of elastic properties on hydrate concentration while keeping the matrix microstructure unchanged.

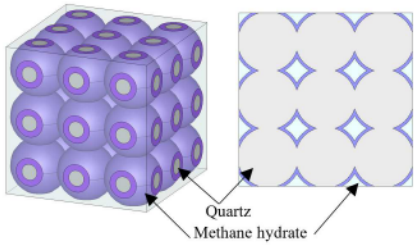

Fig. 1. Schematic illustration of a fragment of the model.

The elastic properties and density of each component were assumed constant and are given in Table I [10].

TABLE I. ELASTIC PROPERTIES USED IN THE MODELLING

Component	Bulk Modulus, GPa	Shear Modulus, GPa	Density, g/cm^3
Quartz	K = 36.6	G = 45	2.65
Water	K_w = 2.25	0	1
Methane Hydrate	K_H = 8.7	G_H = 3.55	0.926

B. Static Approach

To obtain the wave velocities of the heterogeneous sample from the effective elastic moduli, a series of stationary continuum mechanics problems is solved for each sample $\Omega = \Omega_{\text{quartz}} \cup \Omega_{\text{hydrate}} \cup \Omega_{\text{water}} \subset R^3$ in the form:

$$\begin{aligned} &-\nabla \cdot \left(\mathbf{D}(\mathbf{x}) : \nabla_s \mathbf{U}_q(\mathbf{x}) \right) = 0 \ \text{ in } \ \Omega, \\ &\mathbf{U}_q\big|_{\partial\Omega} = \boldsymbol{\xi}_q(\mathbf{x}), \end{aligned} \tag{1}$$

where $\mathbf{D}(\mathbf{x})$ is the fourth-rank stiffness tensor [Pa] in Voigt notation: $\mathbf{D}(\mathbf{x}) = \{d_{ij}\}_{i,j=1..6}$, $\mathbf{U}_q(\mathbf{x})$ is the displacement vector field [m], solved under boundary conditions $\boldsymbol{\xi}_q(\mathbf{x}) = \left(\xi_x^q(\mathbf{x}), \xi_y^q(\mathbf{x}), \xi_z^q(\mathbf{x})\right)^T$ corresponding to uniaxial strains $q = \{xx, yy, zz\}$ and shear $q = \{xy, yz, xz\}$ deformations [11].

The variational formulation of the homogenization problem (1) is posed over the space of kinematically admissible displacements. Let $\mathbf{V}(\Omega)$ be the space of vector-valued functions defined on Ω that satisfy prescribed boundary conditions.

The research was supported by project No. FWZZ-2022-0030 (dynamic approach) and RSF 25-71-10045 (static approach).

The weak form is: Find $\mathbf{U}_q(\mathbf{x}) \in \mathbf{V}(\Omega)$ such that for all test functions $\mathbf{w}(\mathbf{x}) \in \mathbf{V}(\Omega)$,

$$a\left(\mathbf{w}(\mathbf{x}), \mathbf{U}_q(\mathbf{x})\right) = 0, \tag{2}$$

where the bilinear form $a(\square,\square)$ representing the virtual work of internal stresses is defined as:

$$a\left(\mathbf{w}(\mathbf{x}), \mathbf{U}(\mathbf{x})\right) = \int_\Omega \nabla_s \mathbf{w}(\mathbf{x}) : \mathbf{D}(\mathbf{x}) : \nabla_s \mathbf{U}_q(\mathbf{x}) d\Omega. \tag{3}$$

For numerical implementation, this continuous formulation is discretized using the Finite Element Method. The domain Ω is partitioned into a mesh of finite elements, and the solution u is approximated by $\mathbf{U}_q^h(\mathbf{x}) = \sum_{i=1}^n \mathbf{N}_i(\mathbf{x}) \mathbf{u}_i^q$ where $\mathbf{N}_i(\mathbf{x})$ are the vector-valued shape functions and $\mathbf{u}_i^q$ are nodal displacements for n nodes.

The discrete problem leads to the linear system $\mathbf{K}\mathbf{U}^q = \mathbf{F}$, where $\mathbf{K}$ is the global stiffness matrix assembled from element contributions $\mathbf{K}^e = \int_{\Omega^e} \mathbf{B}^T \mathbf{D} \mathbf{B} d\Omega$, with $\mathbf{B}$ containing derivatives of shape functions, $\mathbf{U}^q$ is the vector of nodal displacements, and $\mathbf{F}$ is the load vector consistent with the applied macroscopic strains [11].

The figures below show the stress intensity distributions for a methane hydrate layer thickness of 0.05 mm (Fig. 2) and 0.3 mm (Fig. 3), obtained from solving uniaxial tension problems along the OX axis.

In the model under consideration, it is assumed that the pores are filled with water in addition to methane hydrate. To avoid solving additional hydrodynamic equations, we introduce the assumption that the pores are filled with a material whose shear modulus is close to zero.

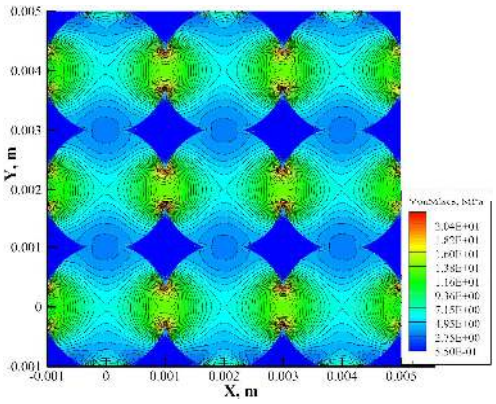

Fig. 2. Von Mises stress in a fragment of a cross-section passing through the centres of quartz grains coated with a 0.05 mm hydrate layer.

Thus, to determine the full effective elastic stiffness tensor $\mathbf{D}_{eff}$, six independent macroscopic strain states are used (e.g., uniaxial tension along the three axes and simple shear in the three planes). After solving the boundary value problem, homogenisation is performed based on the principle of equality of the specific elastic deformation energy of the

homogenised body and the original heterogeneous object (the energy approach) [11], [12].

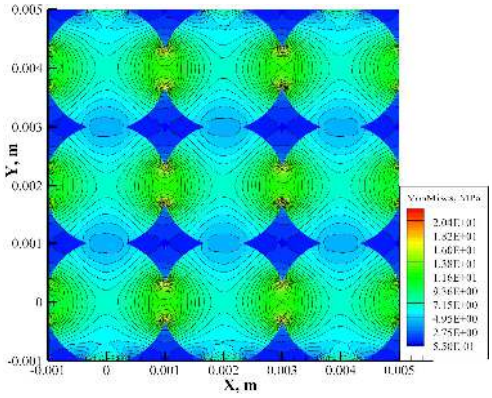

Fig. 3. Von Mises stress in a fragment of a cross-section passing through the centres of quartz grains coated with a 0.3 mm hydrate layer.

Since the sample is isotropic relative to the principal axes, the effective bulk modulus K_{eff} and the effective shear modulus G_{eff} can be calculated from $\mathbf{D}_{eff}$:

$$K_{eff} = \left(\sum_{i,j=1}^{3} d_{ij}\right)/3,\ G_{eff} = \left(\sum_{i=4}^{6} d_{ii}\right)/3. \qquad (4)$$

The effective density ρ_{eff} was calculated using the rule of simple volumetric averaging.

The compressional Vp_{static} and shear Vs_{static} wave velocities can then be obtained using the relations:

$$Vp_{static} = \sqrt{\left(K_{eff} + \frac{4}{3}G_{eff}\right)/\rho_{eff}}, \qquad (5)$$

$$Vs_{static} = \sqrt{G_{eff}/\rho_{eff}}, \qquad (6)$$

C. Dynamic Approach

The dynamic calculation of the $Vp_{dynamic}$ velocity requires solving a full transient problem of elastic wave propagation in a heterogeneous medium (Fig. 4):

$$\nabla\cdot\left(\mathbf{D}(\mathbf{x}):\nabla_S\mathbf{U}(\mathbf{x},t)\right) = \rho(\mathbf{x})\frac{d^2\mathbf{U}(\mathbf{x},t)}{dt^2} \text{ in } \Omega,\ t\in[0,T], \qquad (7)$$

with boundary conditions:

$$\mathbf{U}(\mathbf{x},t)\big|_{\Gamma_{down}} = \mathbf{0}, \qquad (8)$$

$$\boldsymbol{\sigma}(\mathbf{x},t)\cdot\mathbf{n}\big|_{\Gamma_{up}} = \begin{cases} -\mathbf{n}F, & t\le\tau \\ \mathbf{0}, & t>\tau, \end{cases} \qquad (9)$$

$$\boldsymbol{\sigma}(\mathbf{x},t)\cdot\mathbf{n}\big|_{\partial\Omega\setminus\left(\Gamma_{up}\cup\Gamma_{down}\right)} = \mathbf{0}, \qquad (10)$$

and initial conditions:

$$\mathbf{U}(\mathbf{x},t)\big|_{t=0} = \mathbf{0},\ \left.\frac{d\mathbf{U}(\mathbf{x},t)}{dt}\right|_{t=0} = \mathbf{0}, \qquad (11)$$

is the source function with an amplitude of $P=1$ MPa; the source is switched off after a time $\tau=0.2$ mks.

The vertical component of displacement is recorded near the bottom face. The compressional wave velocity $Vp_{dynamic}$ is then determined as the ratio of the sample length L=10 mm to the first-arrival time dt.

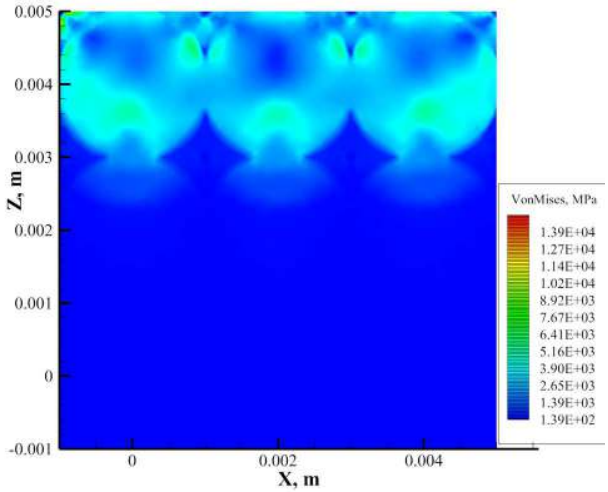

Fig. 4. A snapshot of the Von Mises stress in a fragment of a cross-section passing through the centres of quartz grains coated with a 0.3 mm hydrate layer.

The variational formulation is derived by multiplying the strong form by a test function $\mathbf{w}(\mathbf{x})\in\mathbf{V}(\Omega)$, where $\mathbf{V}(\Omega)$ is an appropriate function space satisfying the essential boundary conditions, and integrating over Ω. The semi-discrete weak form becomes: Find $\mathbf{U}(\mathbf{x},t)\in\mathbf{V}(\Omega)$ such that for all $\mathbf{w}(\mathbf{x})\in\mathbf{V}(\Omega)$ and $t\in[0,T]$,

$$m\left(\mathbf{w}(\mathbf{x}),\frac{d^2\mathbf{U}(\mathbf{x},t)}{dt^2}\right) + a\left(\mathbf{w}(\mathbf{x}),\mathbf{U}(\mathbf{x},t)\right) = l\left(\mathbf{w}(\mathbf{x})\right), \qquad (12)$$

where the bilinear and linear forms are defined as:

$$m\left(\mathbf{w}(\mathbf{x}),\frac{d^2\mathbf{U}(\mathbf{x},t)}{dt^2}\right) = \int_\Omega \rho(\mathbf{x})\mathbf{w}(\mathbf{x})\cdot\frac{d^2\mathbf{U}(\mathbf{x},t)}{dt^2}d\Omega,$$

$$a\left(\mathbf{w}(\mathbf{x}),\mathbf{U}(\mathbf{x},t)\right) = \int_\Omega \nabla_s\mathbf{w}(\mathbf{x}):\mathbf{D}(\mathbf{x}):\nabla_s\mathbf{U}(\mathbf{x},t)\,d\Omega,$$

$$l\left(\mathbf{w}(\mathbf{x})\right) = \int_\Omega \mathbf{w}(\mathbf{x})\cdot\mathbf{F}(\mathbf{x},t)\,d\Omega.$$

For numerical implementation, the spatial discretization using the Finite Element Method leads to the system of ordinary differential equations:

$$\mathbf{M}\,d^2\mathbf{U}(t)/dt^2 + \mathbf{K}\mathbf{U}(t) = \mathbf{F}(t), \qquad (13)$$

where $\mathbf{M}$ is the consistent mass matrix with elements $M_{ij} = \int_\Omega \mathbf{N}_i \cdot \mathbf{N}_j d\Omega$ (the shape functions are the same as in the static case), $\mathbf{K}$ is the stiffness matrix, $\mathbf{U}(t)$ is the vector of nodal displacements, and $\mathbf{F}(t)$ is the load vector. The time integration is performed using the implicit Newmark scheme with parameters β = 0.25 and γ = 0.5, which provides unconditional stability for wave propagation problems.

III. Results

The main results obtained using the developed software package based on the algorithms described above are presented below. Corresponding finite element methods were implemented to solve the systems of equations (1) and (5)-(9). Time resolution in the transient problem was achieved using the Newmark method. All resulting systems of linear algebraic equations were solved using Krylov subspace methods. Verification of the software suite is provided in [12]. The mesh discretisations of the simulated samples comprised approximately 20 million tetrahedra.

A. Dependence of Effective Properties on Hydrate Saturation

A series of static calculations yielded the dependencies of the effective bulk modulus K_{eff} and shear modulus G_{eff} on hydrate saturation. As expected, a monotonic increase in K_{eff} and G_{eff} with increasing hydrate concentration is observed (Fig. 5).

The term "methane hydrate concentration" herein refers to the ratio of the hydrate volume to the total pore space (i.e., the volume of the sample not occupied by the quartz matrix).

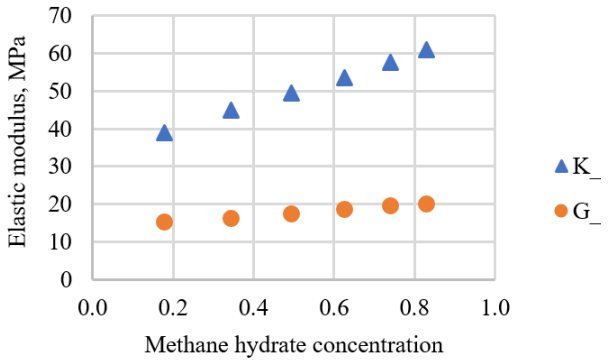

Fig. 5. Dependence of the effective bulk modulus (K_{eff}) and the effective shear modulus (G_{eff}) on the methane hydrate concentration in the pore space.

B. Comparison of Static and Dynamic Velocities

Fig. 6 shows the dependencies of the compressional wave velocity on hydrate saturation, calculated using the two methods. The graph demonstrates a sufficiently high degree of agreement between Vs_{static} and $Vp_{dynamic}$ across the entire saturation range (the relative difference does not exceed 10%). Trend lines (third-degree polynomial) were also fitted to all data sets (Fig. 6).

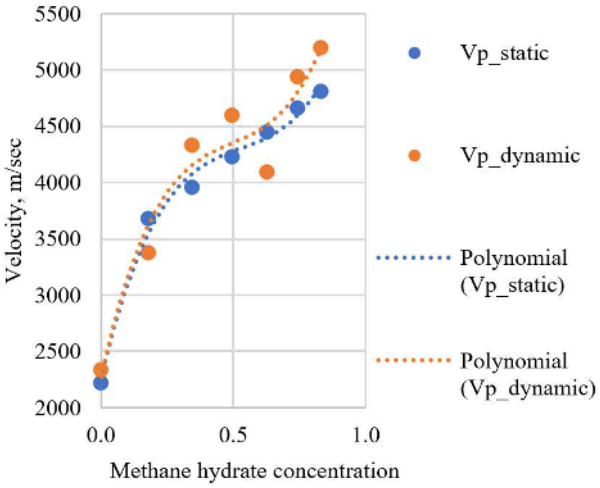

Fig. 6. Comparison of the compressional wave velocity calculated by static (Vp_static) and dynamic (Vp_dynamic) methods.

To compare the numerical modelling results with physical experiments, the absolute velocity values were shifted so that they coincided at zero hydrate saturation. This normalization compensates for the influence of different host matrices in the experimental samples and allows for a direct comparison of the relative effect of hydrate saturation on elastic wave velocities.

A quantitative analysis shows that the deviation of the experimental data points (physical experiments data obtained earlier under the project FUUM-2019-0007 of the Ministry of Science and Higher Education [11]) from the trend line of the calculated results does not exceed 8%. This discrepancy is considered satisfactory and can be attributed to the idealized nature of the numerical model. Specifically, the model assumes a perfect coating of quartz grains by hydrate, which is difficult to achieve consistently in laboratory conditions. The non-ideal and heterogeneous hydrate distribution in real physical samples is likely the primary cause of the data scatter observed in Fig. 7, where significant variations in velocity occur even at similar hydrate saturations. Thus, the developed model provides a reliable upper-bound estimate of the velocity increase for a given hydrate saturation under ideal cementation conditions.

Both calculated curves of relative velocities show satisfactory agreement with data from physical experiments (Fig. 7), obtained earlier under the project FUUM-2019-0007 of the Ministry of Science and Higher Education (Trofimuk Institute of Petroleum Geology and Geophysics SB RAS) [13].

IV. Conclusion

This work presents the results of comprehensive numerical modelling of the effective elastic properties of hydrate-bearing rock using a developed software package based on the finite element method. Both stationary problems for determining static elastic moduli and transient wave problems for the direct calculation of elastic wave propagation velocities were solved.

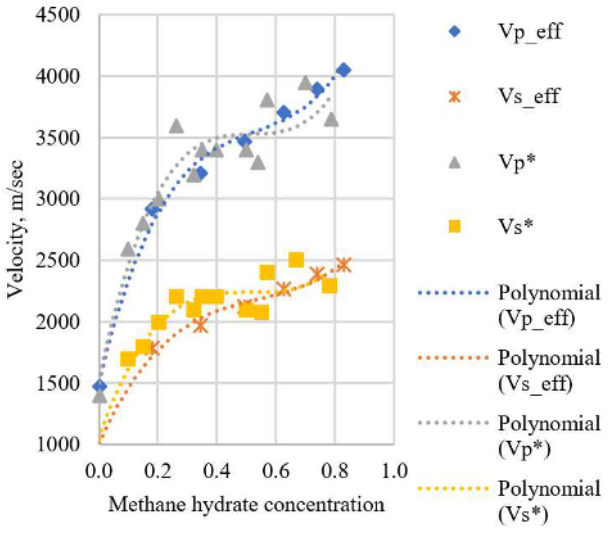

Fig. 7. Comparison of the compressional and shear wave velocities obtained numerically (Vp_eff, Vs_eff) and from laboratory experiments

Correct dependencies of the effective bulk and shear moduli on methane hydrate concentration were obtained, demonstrating the expected monotonic increase with rising saturation.

Satisfactory agreement (with a relative difference not exceeding 10%) was established between the compressional wave velocities calculated via the static moduli and the velocities obtained from direct dynamic modelling. This confirms the adequacy and interchangeability of the two approaches for the used medium model.

Successful comparison with data from physical experiments was conducted. After normalizing the velocities to compensate for differences in the host matrix, the calculated curves demonstrated good qualitative and quantitative agreement with the experimental data (with a relative difference not exceeding 8%), which verifies the proposed numerical methodology.

Thus, the developed computational approach and the obtained results can serve as a reliable basis for constructing and calibrating rock physics models of hydrate-bearing rocks, as well as for predicting their seismic characteristics.

ACKNOWLEDGMENT

The research was supported by project No. FWZZ-2022-0030 (dynamic approach) and RSF 25-71-10045 (static approach).

REFERENCES

[1] V. T. Gudzenko, A. A. Varenichev, and M. P. Gromova, "World economy and gas hydrates," (in Russian), Gornyy Informatsionno-Analiticheskiy Byulleten, no. 10, pp. 43-57, 2018. DOI: 10.25018/0236-1493-2018-10-0-43-57.

[2] A. Rauf, H. M. Faisal, and A. Memon, "Energy resources potential of methane hydrate as potential fuel source," in Proc. 2015 International Field Exploration and Development Conference (IFEDC 2015), Jan. 2015. DOI: 10.1049/cp.2015.0585.

[3] A. D. Duchkov, L. S. Sokolova, M. N. Zheleznyak, and D. E. Ayunov, "To the question about the search fields of methane hydrates in the areas of permafrost distribution," (in Russian), Geofizicheskie Tekhnologii, no. 2, pp. 27-40, 2018. https://doi.org/10.18303/2619-1563-2018-2-3.

[4] A. A. Bocharova and N. V. Shalaeva, "On the possibilities of studying the base of the gas hydrate layer on marine seismic data using adaptive wave field subtraction," (in Russian), Vestnik Moskovskogo Universiteta. Seriya 4: Geologiya, no. 4, pp. 75-77, 2011.

[5] A. S. Pirogova, A. Ye. Chegodaeva, and S. G. Mironyuk, "Study of gas hydrates in the deep-water part of the Sea of Okhotsk using multi-frequency 3D seismic data: Part 1. Methodology," (in Russian), Geofizika, no. 2, pp. 65-75, 2023.

[6] E. I. Mashinsky, "Differences between static and dynamic elastic moduli of rocks: Physical causes," Geology and Geophysics, vol. 44, no. 9, pp. 953-959, 2003.

[7] Z. Guo, X. Wang, J. Jiao, and H. Chen, "Rock Physics Model and Seismic Dispersion and Attenuation in Gas Hydrate-Bearing Sediments," Frontiers in Earth Science, vol. 9, p. 641606, Mar. 2021. DOI: 10.3389/feart.2021.641606.

[8] G. M. S. Gidrão, R. Carrazedo, R. M. Bosse, L. Silvestro, R. Ribeiro, C. F. P. de Souza, "Numerical Modeling of the Dynamic Elastic Modulus of Concrete," Materials (Basel), vol.16, no. 11, pp. 3955, 2023. doi: 10.3390/ma16113955.

[9] E. Norouzi, B. Li, E. Erkmen, "Numerical homogenization of anisotropic static elastic properties of soft mudrocks," Geo-Congress, vol. 2022, pp. 589-598, 2022.

[10] W. F. Waite, W. J. Winters, and D. H. Mason, "Methane hydrate formation in partially water-saturated Ottawa sand," American Mineralogist, vol. 89, pp. 1202-1207, 2004.

[11] A. Yu. Kutishcheva and D. V. Dobrolyubova, "Numerical estimation of the influence of the sample structure on its effective elastic properties," (in Russian), in Proc. INTEREXPO GEO-Siberia, vol. 2, pp. 152-159, 2024.

[12] E. P. Shurina, N. B. Itkina, N. V. Shtabel, E. I. Shtanko, A. Yu. Kutishcheva, S. I. Markov, D. V. Dobrolubova "Determination of thermal, stiffness and electrical effective tensors in composite media, " Journal of Computational and Applied Mathematics, vol. 409. pp. 114009, 2022

[13] E.I. Shtanko, "Creation of a unified mathematical, algorithmic and software structure ensuring the adoption of discriminating technological decisions in the design of modern measuring equipment for geophysical, biological engineering applications," (in Russian), Final Report on Research Work for 2021, Project no. FUUM-2019-0007. INGG SO RAN, P.147, 2021.